














## Multiple differential electron spectra from detachment in collisions of 30–300-keV anions with atoms and molecules

M. Schulz , F. Herrmann , W. Zhang , D. V. Chicharro , A. Dorn , M. Grieser , F. Grussie , H. Kreckel ,  
O. Novotny , F. Trost , A. Wolf , T. Pfeifer , C. D. Schröter , and R. Moshhammer  
*Max-Planck-Institute for Nuclear Physics, Saupfercheckweg 1, D-69117 Heidelberg, Germany*



(Received 8 May 2024; accepted 12 August 2024; published 27 August 2024)

We have measured triple differential momentum distributions for electron detachment in collisions of 30- and 300-keV anions ( $C^-$  and  $Si^-$ ) with atoms and molecules (He, Ar, and  $N_2$ ). The entire angular range of the ejected electrons was covered. The binary encounter ring, well known from positive ion-atom collisions, was observed in most cases. In a quasifree-electron scattering model this structure represents elastic scattering of the active electron from the target. However, especially for the slowest projectiles, this model fails to reproduce the angular distributions. In this regime it is probably necessary to use quasimolecular models to describe the collision. Indications for a projectile cusp are observed, implying that excitation-induced dipole moments in the ion projectile may be important.

DOI: [10.1103/PhysRevA.110.022818](https://doi.org/10.1103/PhysRevA.110.022818)

### I. INTRODUCTION

One of the fundamental processes occurring in atomic collisions is the removal of an electron from one of the collision partners. Studies of such processes are particularly suitable to advance our understanding of the few-body problem. The essence of the few-body problem is that the Schrödinger equation is not solvable in closed form for more than two mutually interacting particles even if the forces acting within any pair of two particles in the system are precisely known (e.g., [1,2]). Electron removal processes, i.e., ionization of the target or detachment from the projectile, are especially subjected to this problem because, in contrast to excitation or capture, the final state involves three unbound particles. Two factors which can significantly contribute to the difficulties in solving the few-body problem are (a) an incomplete understanding of the underlying forces and (b) the long-range nature of the underlying forces. One well-known approach to solving the few-body problem is based on the Faddeev equations [3]. It was originally designed for short-range forces, which should make it well applicable to nuclear systems. On the other hand, our understanding of the nuclear force is still rather incomplete. The essentially complete understanding that we have about the Coulomb force acting between two charged particles may make atomic systems better candidates for studies of the few-body problem.

Ideally, one would study systems in which the underlying two-particle forces are completely understood short-range forces. Of course, such a system does not exist. However, an

approximate realization may be offered by anions colliding with neutral atoms or molecules. Because the forces acting within pairs of particles are well known, the static structure of the collision partners can often be calculated accurately using numeric methods like the Hartree-Fock approach. At the same time, if an electron is removed from the projectile the residual collision partners are both neutral. Therefore, the forces leading to the transition and acting on the ejected electron can be reasonably modeled as short-range forces. This can significantly reduce the required computational efforts because the spatial integrals of the transition amplitude can be reduced to much smaller dimensions compared to collisions involving charged particles in the final state. A well-known manifestation of the long-range nature of the Coulomb force acting between charged particles is the occurrence of the so-called cusp peak in the ejected electron spectra [4]. It is due to a transition of the electron from a bound state of one collision partner to a low-lying continuum state of either the same (electron loss to the continuum) or the other partner (electron capture to the continuum). The long-range interaction of the latter with the electron gives the cusp peak its eponymous shape. The very high sensitivity of the description of cusp electrons on the details of the theoretical model has been demonstrated [5].

Total cross sections for detachment in anion-atom collisions have been studied extensively (e.g., [6–17]). At small collision velocities these data can be reasonably well described within a quasimolecular picture [18] and by models using the zero-range potential approximation [19–21]. At intermediate and high velocities remarkable success was achieved by treating the active electron on the projectile as quasifree [15,16]. The detachment cross sections were obtained by convoluting the elastic scattering cross section for free electrons [22] with the Compton profile on the projectile. However, it is rather challenging to develop models which are applicable for all collision velocities.

---

Published by the American Physical Society under the terms of the [Creative Commons Attribution 4.0 International](https://creativecommons.org/licenses/by/4.0/) license. Further distribution of this work must maintain attribution to the author(s) and the published article's title, journal citation, and DOI. Open access publication funded by Max Planck Society.

Macek *et al.* [23] have presented such a model, based on the zero-range approximation, to calculate triple differential momentum distributions of electrons ejected in detachment in ion-atom collisions. For relatively fast collisions ( $v_p = 10$  a.u., where a.u. denotes atomic units) they found some of the features that are well known for ionization of the target atom by positively charged ion impact: the projectile cusp, occurring at  $v_z/v_p = 1$  in the laboratory frame (corresponding to the target cusp in the case of target ionization [24]), the target cusp occurring at  $v_z/v_p = 0$ , and a ring extending from  $v_z/v_p = -1$  to 1 due to binary encounter collisions. Here,  $v_z$  and  $v_p$  are the longitudinal electron speed and the projectile speed, respectively, and a.u. denotes atomic units. Binary encounter refers to a direct first-order interaction between the active electron and the target. For slow collisions ( $v_p = 0.1$  a.u.) the binary encounter ring disappeared and the projectile and target cusps merged into a single peak.

Initially, the occurrence of cusp structures was associated with a long-range potential. However, as pointed out by Liu and Starace [25] and Barrachina [26], even for a short-range potential cusp peaks can be significant if the residual neutralized projectile is left in an excited state. Due to the degeneracy in the orbital angular momentum quantum number the superposition of two states of opposite parity can lead to an electric dipole moment. In most cases, even the ground state can be polarized by the field of the target, however, the transient dipole moment only survives for the duration of the collision (typically a fraction of a fs). In the case of excitation to a superposition of degenerate states this lifetime is enhanced by several orders of magnitude. Due to the small binding energies of anions such polarization effects are further enhanced. An interaction of the detached electron with the induced dipole moment can result in a cusp-shaped peak. It was further suggested that these peaks could be present, due to virtual excited states on the projectile, even without any permanent dipole moments [27]. Cusp structures were indeed experimentally confirmed by Viktor *et al.* [28] in 85-keV  $H^- + He$  collisions.

Two features which were observed in measured ejected electron spectra [29,30] were not discussed in the work of Macek *et al.* [23]: (a) low-energy electrons (in the rest frame of the emitter) resulting from direct removal and (b) resonant electron emission due to doubly excited intermediate states on the emitter. The former is distinguished from cusp electrons by the shape of the energy spectrum, which is much broader than the characteristic cusp shape. Furthermore, it does not rely on the presence of a long-range force, an electric dipole moment, or virtual states.

Here, we present measured momentum distributions of electrons detached from various anions colliding with various target atoms and molecules at speeds ranging from 0.224 to 1.0 a.u. These spectra are equivalent to those calculated by Macek *et al.*, although we will present them in a different differential form. Nevertheless, a direct quantitative comparison with these theoretical results is not possible because Macek *et al.* did not specify (except for the projectile speed) the collision system for which they performed the calculations. Qualitatively, we observe some of the features predicted by Macek *et al.* while others are absent in the data. Furthermore, we did not find any indications for resonant states on the projectiles contributing to electron detachment. However, we did

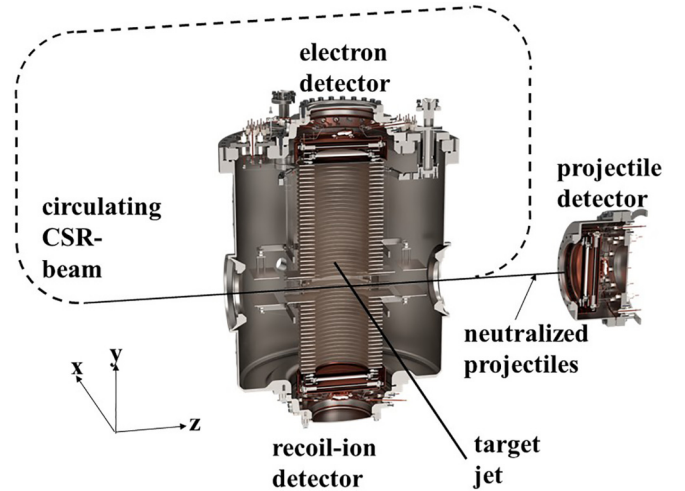


FIG. 1. Experimental setup. The ReMi spectrometer consists of the ring-shaped electrodes and the electron and recoil-ion detectors (not used in the present project) on top and bottom of the spectrometer. Both detectors were set in coincidence with the neutralized projectile detector.

observe clear signatures for a strong resonance on the target in collisions with  $N_2$ . The quasifree electron scattering model [15,16], which very well describes total cross sections, cannot reproduce our multiple differential data even qualitatively.

## II. EXPERIMENTAL SETUP

The experiment (see schematic setup in Fig. 1) was performed at the Cryogenic Storage Ring CSR [31] at the Max-Planck-Institute for nuclear physics in Heidelberg. Anions ( $C^-$ ,  $C_2^-$ , and  $Si^-$ ) were produced with a sputter source and injected into the CSR. There, they were stored at an energy ranging from 30 to 300 keV. Depending on the ion and projectile energy the storage time varied between 30 and 60 sec. One important feature of the CSR is the extremely good vacuum of less than  $10^{-12}$  mbar. As a result, data could be taken essentially free of background from collisions with the residual gas. One detrimental feature is the large beam size of about 1 cm, which is the price to be paid for a very good transverse momentum sharpness of about  $\Delta p_{tr}/p = 10^{-4}$ . The projectiles neutralized in the collision with the target were separated from the charged projectiles by the first of the electrostatic deflectors after the target region keeping the beam in the CSR (not shown in Fig. 1). They were then detected by a microchannel plate (MCP) detector with a diameter of 12 cm equipped with a two-dimensional position-sensitive delay-line anode.

The projectile beam was crossed at  $90^\circ$  with a very cold beam ( $T \approx 1$  K) of neutral atoms (He or Ar) or molecules ( $N_2$ ) from a supersonic jet. The ejected electrons (and recoil ions produced by target ionization, although not used in this analysis) were momentum-analyzed by means of a reaction microscope (ReMi), which is schematically shown in Fig. 1, and detected by MCP detectors identical to the projectile detector. Here, we focus on electron detachment; the data on accompanying target ionization will be reported in a forthcoming article. The operation of a ReMi in the CSR

requires special design characteristics because of the very low temperature of the CSR ( $T < 10$  K), the demanding vacuum requirements, and the need of an obstruction-free passage of the stored ions. The proper operation of the spectrometer and the detectors under these conditions was confirmed by crossing the projectile beam with a laser beam (photon energy of 1.5 eV) and measuring electrons ejected in photodetachment. Since this process leads to discrete electron energies this also allowed us to calibrate the spectrometer. The details of the ReMi will be reported in a forthcoming paper. Here, it suffices to state that the basic concepts of momentum-analyzing the electrons and recoil ions are the same as in a “standard” ReMi [32,33]. In the present context, the most important difference is that in the CSR design the particles are extracted transversely relative to the ion beam by a combination of weak uniform electric and magnetic fields, which forces the electrons into cyclotron motion. As a result, electrons with sufficiently small momentum (typically 1–1.5 a.u.) are confined to the size of the detector. All three detectors were set in coincidence with each other.

The two momentum components in the plane of the detectors (see coordinate system in Fig. 1) are obtained from the position information and the component in the direction of the extraction field from the time of flight which, in turn, is contained in the coincidence time. One difficulty concerns the determination of the electron momentum component in the  $x$  direction, which is given by the target beam direction. The large ion beam size leads to a large overlap with the target beam which would, if not corrected for, result in a poor momentum resolution. Therefore, the position of the neutralized projectiles was measured and the departure from the centroid trajectory of the ions could be determined and subtracted from the electron position. The departure from the centroid trajectory caused by the scattering in the collision and the anion beam divergence is negligible. The momentum components in the  $y$  and  $z$  directions (defined by the recoil-ion extraction field and by the ion beam, respectively) are not affected by this problem because they are perpendicular to the target beam direction, and its width in both transverse directions is less than 1 mm.

### III. RESULTS AND DISCUSSION

To the extent possible, the data will be presented in the order of decreasing projectile speed, i.e., from  $v_p = 1.0$  a.u. for 300-keV  $C^-$  down to  $v_p = 0.22$  a.u. for 30-keV  $C_2^-$ . We will first analyze two-dimensional momentum distributions of the ejected electrons in the  $xz$  plane with a condition  $|p_{ely}| < 0.05$  a.u. (where  $p_{ely}$  denotes the electron momentum in the  $y$  direction). By this condition the distance of any data point from the origin in the displayed plane represents the magnitude of the electron momentum. Later, we will discuss the angular electron distributions for fixed electron energies. We will start with the data for atomic targets and at the end briefly address the only molecular target for which we took data, namely  $N_2$ . The two-dimensional momentum distributions are shown in Figs. 2–6 for 300-keV  $C^- + Ar$  (Fig. 2), for 300-keV  $Si^-$  colliding with He (Fig. 3) and Ar (Fig. 4), as well as for 30-keV  $C^-$  (Fig. 5) and  $C_2^- + Ar$  (Fig. 6). The arrows show the direction of the incoming projectile ion beam, and

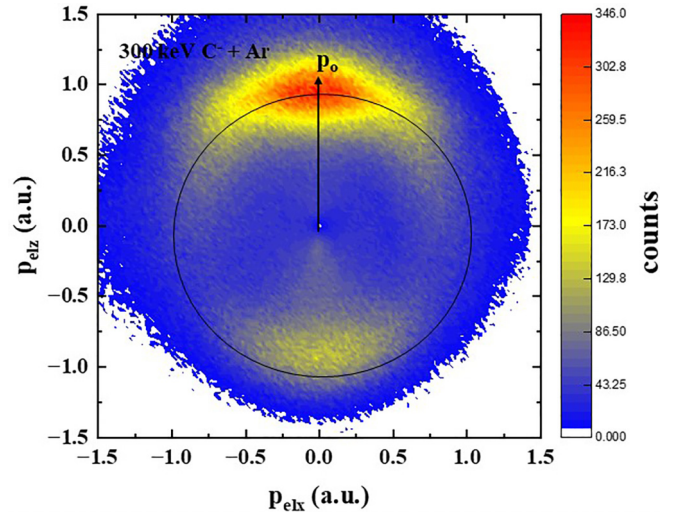


FIG. 2. Two-dimensional momentum distribution in the  $xz$  plane of electrons detached in 300-keV  $C^- + Ar$  collisions with a condition on the  $y$  component at  $0 \pm 0.05$  a.u. Since the spectrum was multiplied by the magnitude of the momentum, the count rate is directly proportional to  $d^3\sigma/d\Omega^2dE$ . The circle indicates the expected location of the binary encounter ring.

the circles indicate where the electron speed is equal to the projectile speed. We started the analysis with spectra which represent triple differential cross sections (TDCSs)  $d^3\sigma/dp^3$  in Cartesian coordinates, which, after transforming using the Jacobi determinant, are equal to  $1/p d^3\sigma/d\Omega^2dE$ . The Cartesian momentum spectra were multiplied by the magnitude of the electron momentum in order to present  $d^3\sigma/d\Omega^2dE$ . The spectra should show left/right symmetry with respect to the projectile beam axis. The observed deviations from this symmetry are due to detection imperfections.

All spectra exhibit a pronounced ringlike shape, which for a projectile energy of 300 keV ( $v_p = 1.0$  and 0.655 a.u. for  $C^-$  and  $Si^-$ , respectively) has a radius close to the projectile speed, while for 30 keV the ring is significantly larger. In addition, the ring shows a substructure, where in most

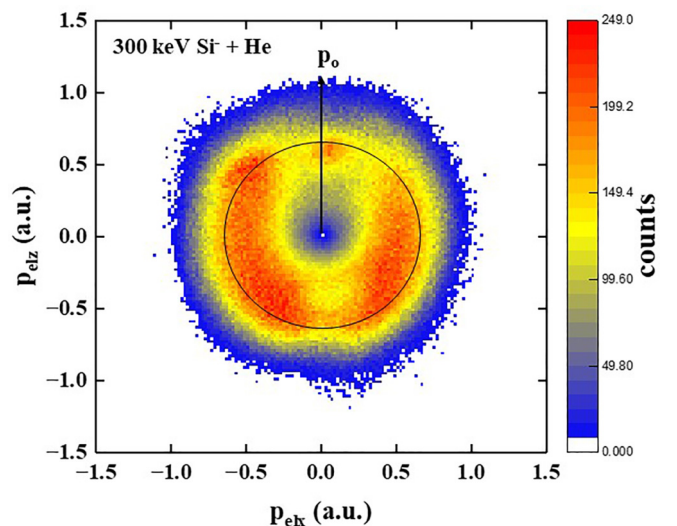
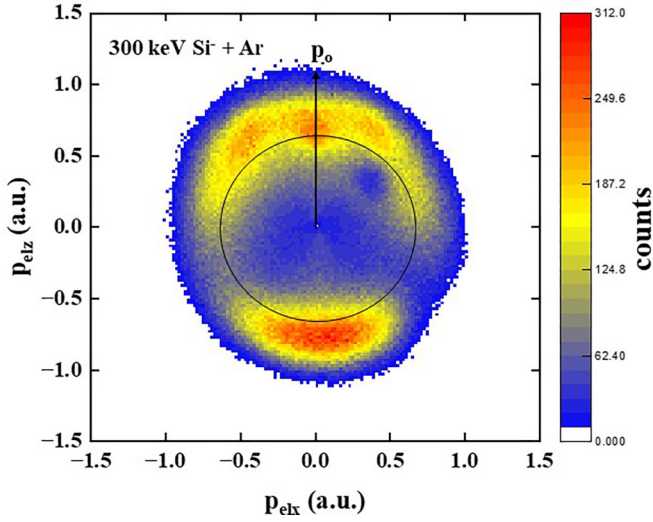


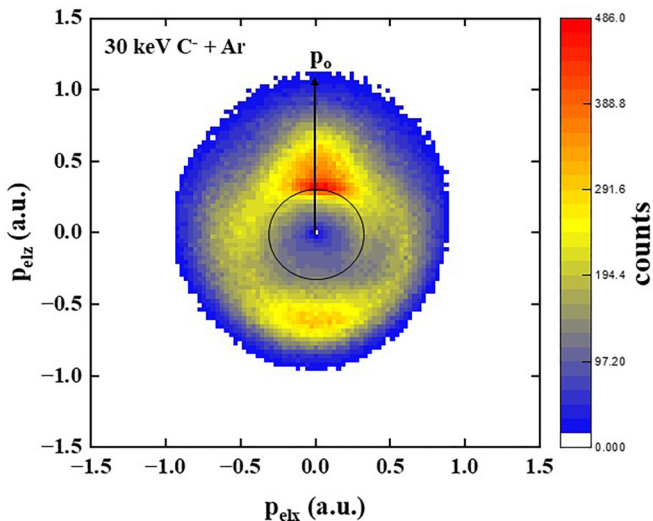
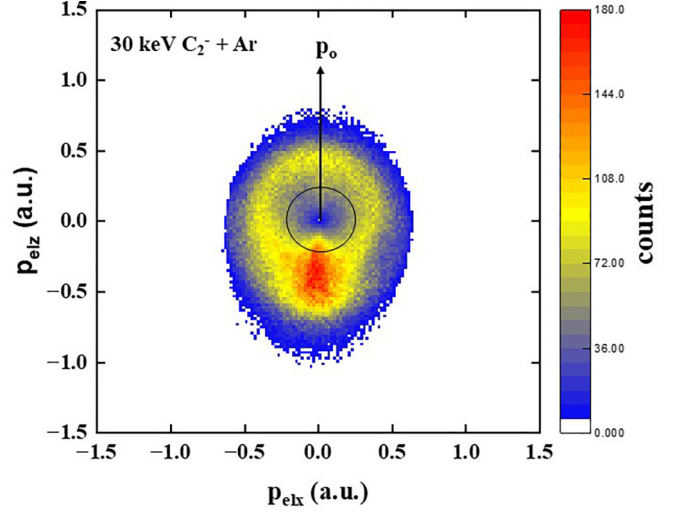
FIG. 3. Same as Fig. 2 for 300-keV  $Si^- + He$  collisions.



FIG. 4. Same as Fig. 2 for 300-keV  $\text{Si}^- + \text{Ar}$  collisions.

cases strong maxima occur in the forward and/or backward direction. Only for the He target (Fig. 3) are such maxima most prominent perpendicular to the beam axis. In the case of  $\text{Si}^- + \text{Ar}$  collisions (Fig. 4) a triple peak structure is seen in the forward direction, and a structure similar in shape to the center peak is also observed for the He target. We will discuss this substructure further when we analyze the triple differential angular distributions of the electrons with fixed energies and compare them to the quasifree electron scattering model. First, we will qualitatively compare our results to the calculations of Macek *et al.* [23].

As mentioned earlier, at large projectile speeds ( $v_p = 10$  a.u.) these calculations reveal the binary encounter ring [see Fig. 1(c) of [23]], with radius  $v_p$ , and sharp peak structures at  $v_z/v_p = 0$  and 1, respectively, in the laboratory frame (note that Macek *et al.* presented their results in the center-of-mass frame). The radius of the predicted binary encounter ring is consistent with the ringlike structure observed in the experiment for the fast projectiles ( $v_p = 0.655$  a.u. for  $\text{Si}^-$  and

FIG. 5. Same as Fig. 2 for 30-keV  $\text{C}^- + \text{Ar}$  collisions.FIG. 6. Same as Fig. 2 for 30-keV  $\text{C}_2^- + \text{Ar}$  collisions.

1.0 a.u. for  $\text{C}^-$ ). Not surprisingly, there are large quantitative differences because the projectile speeds differ by an order of magnitude between experiment and theory. Nevertheless, it seems reasonable to interpret the ring structure as due to binary collisions between the target atom and the active electron on the projectile ion.

The existence of maxima in the forward direction on the rings is expected and relatively easy to understand as an ejection of very slow electrons in the projectile frame. This is precisely what has been observed in other experiments (e.g., [34]) on target ionization by positively charged ion impact in the target frame. What is not obvious is the shape to be expected for this peak structure. As mentioned earlier, in the presence of a long-range potential or a permanent electric dipole moment, induced by excitation of a second electron, cusplike structures with a narrow width are expected. In the data for 300-keV  $\text{C}^-$  impact (Fig. 2), however, we observe a broad structure unlike the cusp peak predicted by Macek *et al.* In contrast, in the data for the  $\text{Si}^-$  projectiles (for both He and Ar, Figs. 3 and 4) the peak in the forward direction comes closer to the expected narrow width and, in the case of the Ar target, is well separated from the accompanying side peaks. These  $\text{Si}^-$  data are thus consistent with the presence of a projectile cusp. However, further down we will also consider whether this forward structure can be explained within the quasifree electron scattering model. If the cusp interpretation is correct, this could imply that  $\text{Si}^-$  attains an electric dipole moment in the collision and  $\text{C}^-$  does not. However, we cannot rule out the possibility that in the case of the  $\text{C}^-$  projectiles the cusp is simply masked by the broader distribution from forward electrons which are not affected by a dipole moment.

A rather different picture emerges for 30-keV  $\text{C}^-$  and  $\text{C}_2^-$  projectile ions ( $v_p = 0.317$  and  $0.224$  a.u., Figs. 5 and 6). Here, the ring has a radius of about twice the projectile speed, and maxima in the forward or backward direction extend well beyond the ring. Furthermore, for this projectile, just exchanging  $\text{C}^-$  and  $\text{C}_2^-$  prompts the momentum spectra to become near mirror images of each other. The ring can therefore not be explained by binary encounter electrons. Indeed, Macek *et al.* concluded that the binary encounter ring completely

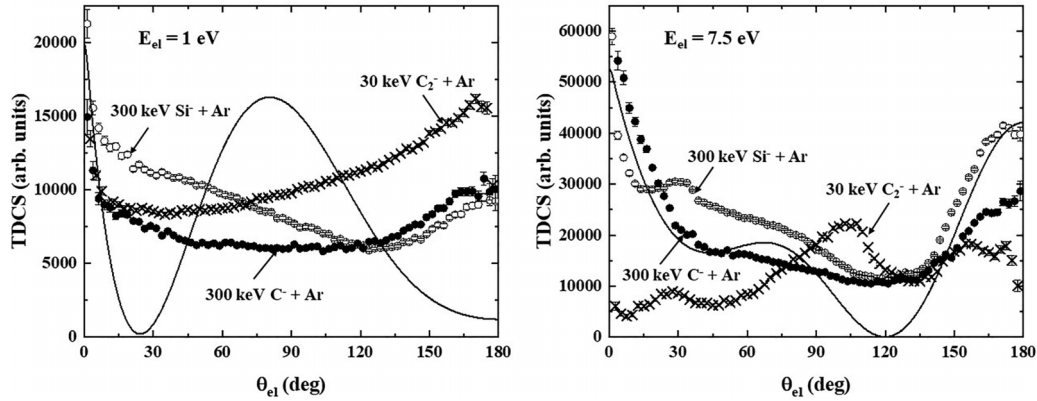


FIG. 7. Triple differential angular distributions of electrons detached in 300-keV  $C^- + Ar$  collisions (closed circles), 300-keV  $Si^- + Ar$  collisions (open circles), and for 30-keV  $C_2^- + Ar$  collisions (crosses). The left panel shows the data for 1 eV and the right panel for 7.5 eV. The curves show calculated differential elastic scattering cross sections for free electrons [39].

disappears at very small  $v_p$ . Instead, they found, like the experiment, a ringlike shape at  $v_{el}/v_p \gg 1$ . Furthermore, in their calculation the projectile and target cusps merge into a single peak at  $v_z/v_p = 0.5$ . Once again it should be noted that in the experiment  $v_p$  was very different from the one used in theory; this time it was larger by more than a factor of 2. It appears that the mechanisms explaining the features observed in target ionization by positively charged ion impact do not always provide an adequate picture to describe detachment from negative ions at very small  $v_p$ . A possible alternative explanation is based on a quasimolecular picture. For example, our data show some resemblance to momentum distributions which were recorded by Schmidt *et al.* [35] for electrons ejected in transfer ionization in slow  $He^{2+} + He$  collisions. They found that the properties of the transient quasimolecular state formed during the collision (e.g., its parity) are mapped into the continuum.

The excitation of the projectile anion to autodetaching resonances, as observed, e.g., in [29,30], should lead to characteristic features in the electron momentum spectra. Since the autodetachment energy is fixed in the projectile frame, the momenta of the ejected electrons would fall on a circle with a radius representing their momentum in the projectile frame centered on the projectile velocity. We did not observe any such structure for any of the collision systems. On the other hand, Balling *et al.* [36] did find resonances in photodetachment of  $Si^-$  and in production of  $Si^+$  in an electron energy range accessible to our experiment. One conceivable reason for this difference could be that the lifetime of the autodetaching state could be long compared to the transit time of the electrons in the spectrometer of about 100–200 ns. However, the lifetime of the intermediate state of  $Si^-$  observed by Balling *et al.* is about 1 fs [36] so that it should have been easily observable with our spectrometer. Furthermore, the projectile detector is sufficiently large to collect essentially all scattering angles so that resonances are not suppressed by favoring distant collisions. Therefore, these differences are likely not due to an experimental artifact, but rather reflect true differences in the transition dynamics between photon and ion impact. However, we cannot rule out the possibility that for other ions, like, e.g.,  $C^-$ , the lifetime of the autodetaching state may be long compared to the transit time of the electrons.

We now return to the substructure occurring along the angular direction on the ring interpreted as a binary encounter ring in the spectrum for 300-keV  $Si^- + Ar$  collisions (Fig. 4). One possible explanation is based on the quasifree electron scattering model. Here, the binding energy of the weakly bound electron is neglected and the collision is viewed as elastic scattering between the electron, moving at the projectile speed, and the target atom. In this model, such events are expected to lie on the binary encounter ring in the momentum spectra of Figs. 2–4. Differential cross sections for truly free electrons have been measured extensively (for reviews see [37,38]). However, experimental multiple differential spectra of electrons detached from *anions* are rare and limited to a narrow range of emission angles (e.g., [29,30]). In contrast, in the present article we report comprehensive TDCS  $d^3\sigma(E, \theta)/d\Omega^2 dE$  covering the entire angular range 0–180°. These are plotted in Fig. 7 for 300-keV  $C^-$  (closed circles) and  $Si^-$  (open circles) and for 30-keV  $C_2^-$  (crosses) colliding with Ar. The left panel shows the data for an electron energy of 1 eV ( $p_e = 0.27$  a.u.) and the right panel for 7.5 eV ( $p_e = 0.74$  a.u.). Here, our interest is focused on the shape of the angular dependence and the data sets for the two electron energies were not normalized relative to each other. Likewise, the theoretical cross sections were adjusted by an arbitrary factor to make the average magnitude similar to the experimental data.

Within the quasifree electron model, an electron energy different from the projectile energy reduced to the electron mass is due to the vector sum of the electron velocity in its initial bound state and the projectile velocity. The ejected electron has the same energy as the incoming electron. For a given target atom and electron energy the differential cross section in first-order approximation should thus neither depend on the ion species nor on the ion speed. However, a comparison between the data for the Ar target reveals large and qualitative differences in the cross sections for the same electron energy. The differences between the two data sets for a projectile energy of 300 keV are considerable, but still relatively moderate. However, the TDCS for 30-keV  $C_2^- + Ar$  do not bear any resemblance at all to the 300-keV data. Here, even a pronounced oscillatory behavior is found in the angular distribution for 7.5 eV. To some extent, differences between

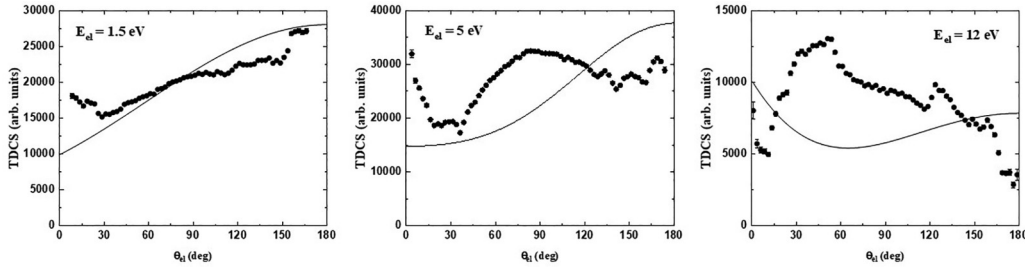


FIG. 8. Same as Fig. 7 for 300-keV  $\text{Si}^- + \text{He}$  collisions and electron energies as indicated by the insets.

the TDCS for different ions can be explained by the initial momentum distribution of the electron in its bound state of the projectile. However, differences of such magnitude and of such qualitative nature may serve as a first hint for the limitations of the quasifree electron scattering model.

The solid curves in Fig. 7 show calculations of differential cross sections for elastic scattering of electrons with an energy equal to the ejected electron energies analyzed in our data [39]. At a projectile energy of 300 keV and an electron energy of 7.5 eV there is qualitative agreement in the case of the  $\text{Si}^-$  ions and fairly good agreement for the  $\text{C}^-$  ions. However, in both cases large differences are observed for 1 eV. In spite of the generally rather poor agreement, in most cases the calculations reproduce the very sharp increase of the cross sections in the forward direction. Therefore, the sharp maxima which we observed for the  $\text{Si}^-$  projectiles in the ejected electron momentum spectra do not necessarily represent cusp structures, but could simply reflect the nature of the elastic scattering process.

For the 30-keV ions the differences are dramatic even on a qualitative level. Based on the comparison with the data for the 300-keV ions one could argue that the quasifree electron model works reasonably well at large collision and electron energies. A gradual failure with a decrease in both energies would perhaps not be too surprising because of the increasing relative importance of the Compton profile of the initial-state electron. However, even for 300-keV  $\text{Si}^- + \text{He}$  the elastic scattering cross sections do not at all reproduce the data, which are shown in Fig. 8. Interestingly, here the differences seem to even get larger with increasing electron energy.

The large differences between the calculations for He and Ar show that the differences between the detachment data for these two targets can at least partly be explained by the target structure. Nevertheless, the enormous differences between the elastic scattering and detachment cross sections also demonstrate that the quasi-free electron model, which works very well for total cross sections and for fast collisions, collapses on the differential level at small projectile speeds. Several contributing factors to this failure are conceivable. First, properly accounting for the initial momentum distribution of the electron on the ion may be significantly more complex than merely convoluting the cross sections with the Compton profile. Second, the interaction of the ejected electron with the residual projectile could be important, especially if it possesses an electric dipole moment. The resulting structures, like cusp peaks, could sensitively affect the cross sections. Third, resonances due to excitation of the projectile ion may be present. Although we could not identify any autodetachment

lines, we may have missed them due to their very narrow width well beyond our experimental resolution (about 0.1 a.u. full width at half maximum in momentum). Finally, quasimolecular effects are likely to play an important role especially at small projectile speeds. Quantum-mechanical interference phenomena are known to be prominent in such transient molecules formed during the collision (e.g., [40,41]). The pronounced oscillations which we observed for the 30-keV  $\text{C}_2^-$  projectiles are likely caused by such interference effects.

Finally, we briefly discuss TDCSs which we measured for 300-keV  $\text{Si}^-$  collisions with a molecular target, namely  $\text{N}_2$ . The electron momentum distribution in the  $xz$  plane for  $p_y = 0 \pm 0.05$  a.u. is shown in Fig. 9. Here, too, a ringlike shape is clearly visible. However, there are two important differences to the data for He and Ar: first, the ring has a smaller radius than  $v_p$  and it can thus not be interpreted as the binary encounter ring. Second, except for the forward direction within  $20^\circ$ , the ring has a fairly uniform angular distribution. The radius corresponds to an electron energy of about 2.3 eV. In this energy region a series of closely lying resonances is known to exist in the case of elastic electron scattering [42–44]. It can thus be safely concluded that this ring represents resonant quasifree scattering of the detached electron from the target. However, this resonance is significantly broadened by vibronic excitation in addition to the electronic transition [44], which unfortunately we cannot resolve. A halo, which is more intense in the forward direction,

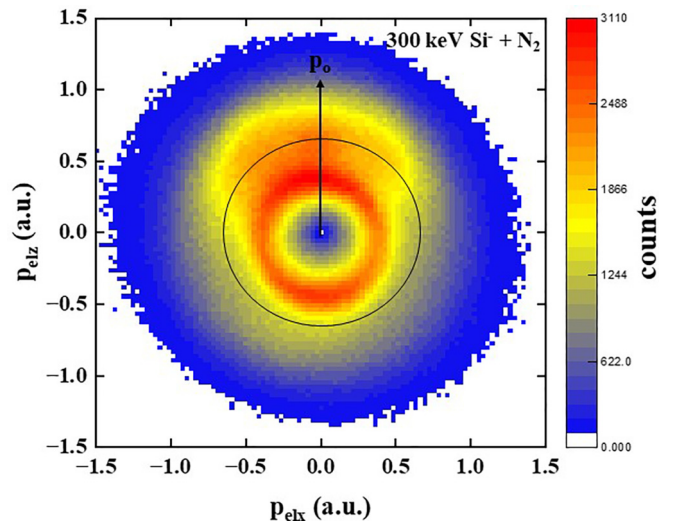


FIG. 9. Same as Fig. 2 for 300-keV  $\text{Si}^- + \text{N}_2$  collisions.



can be seen adjacent to the ring and it is centered close to the projectile speed. We therefore interpret this halo as the binary encounter ring, which is not fully separated from the resonance.

#### IV. CONCLUSIONS

We have measured triple differential momentum distributions of electrons detached in collisions of anions at speeds ranging from 0.224 to 1.0 a.u. with various atomic and molecular targets. From these spectra we also extracted angular distributions of the ejected electrons with fixed energy covering the complete range 0–180°. The results were compared to calculations based on the zero-range potential approximation (qualitatively, because no collision system was specified in the theoretical publication) and to the quasifree electron scattering model.

The zero-range potential calculations predict similar features in the detachment spectra as are well known for target ionization by positively charged ion impact. In our data, only the binary encounter ring is conclusively verified. In some cases, we observed structures in the projectile beam direction which are consistent, but not conclusively confirmed, with a projectile cusp. Considering the absence of a long-range force in the final channel of the collision, the existence of

a cusp would hint at the presence of an electric dipole moment induced by excitation of at least a second electron on the respective collision partner. Therefore, excitation of the projectile ion may play an important role.

The quasifree electron scattering model, which works very well to describe total cross sections for fast ions, still yields reasonable agreement with the present differential data for an Ar target at high projectile speed and large electron energy. However, major differences are found at small electron energies and the model completely collapses for slow projectiles and for a He target. It seems likely that for the small projectile energies the cross sections are strongly affected by quasimolecular couplings. For the slowest projectiles we observe pronounced oscillating patterns which are likely due to quantum-mechanical interference. Final conclusions have to await advanced theoretical calculations of the collision dynamics and of the structure of the specific anionic projectiles and atomic and molecular targets.

#### ACKNOWLEDGMENTS

Financial support by the Max-Planck Society is acknowledged. M.S. is grateful for support from the National Science Foundation under Grant No. PHY-2011307.

- 
- [1] T. N. Rescigno, M. Baertschy, W. Isaacs, and C. McCurdy, *Science* **286**, 2474 (1999).
  - [2] M. Schulz, R. Moshhammer, D. Fischer, H. Kollmus, D. Madison, S. Jones, and J. Ullrich, *Nature (London)* **422**, 48 (2003).
  - [3] L. D. Faddeev and S. P. Merkuriev, *Quantum Scattering Theory for Several Particle Systems* (Kluwer, Dordrecht, 1993).
  - [4] G. B. Crooks and M. E. Rudd, *Phys. Rev. Lett.* **25**, 1599 (1970).
  - [5] M. Dhital, S. Bastola, A. Silvus, J. Davis, B. R. Lamichhane, E. Ali, M. F. Ciappina, R. Lomsadze, A. Hasan, D. H. Madison, and M. Schulz, *Phys. Rev. A* **102**, 032818 (2020).
  - [6] A. K. Edwards, in *The Physics of Electronic and Atomic Collisions*, edited by J. S. Risley and R. Geballe (University of Washington, Seattle, 1975), p. 790.
  - [7] V. A. Esaulov, *Ann. Phys. Paris* **11**, 493 (1986).
  - [8] D. J. Pegg, *Rep. Prog. Phys.* **67**, 857 (2004).
  - [9] F. Zappa, G. Jalbert, L. F. S. Coelho, A. B. Rocha, S. D. Magalhães, and N. V. de Castro Faria, *Phys. Rev. A* **69**, 012703 (2004).
  - [10] H. Luna, F. Zappa, M. H. P. Martins, S. D. Magalhães, G. Jalbert, L. F. S. Coelho, and N. V. de Castro Faria, *Phys. Rev. A* **63**, 052716 (2001).
  - [11] B. Hird and F. Rahman, *Phys. Rev. A* **26**, 3108 (1982).
  - [12] N. Andersen, T. Andersen, L. Jepsen, and J. Macek, *J. Phys. B* **17**, 2281 (1984).
  - [13] J. S. Risley, *Phys. Rev. A* **10**, 731 (1974).
  - [14] G. Mei, Y. En-Bo, L. Yong, Z. Xue-Mei, and L. Fu-Quan, *Chin. Phys. Lett.* **23**, 3253 (2006).
  - [15] G. Jalbert, W. Wolff, S. D. Magalhães, and N. V. de Castro Faria, *Phys. Rev. A* **77**, 012722 (2008).
  - [16] G. M. Sigaud, *J. Phys. B* **41**, 015205 (2007).
  - [17] T. Andersen, *Phys. Rep.* **394**, 157 (2004).
  - [18] J. S. Risley, in *Proceedings of the 11th International Conference on the Physics of Electronic and Atomic Collisions*, Kyoto, 1979, edited by N. Oda and K. Takayanagi (North-Holland, Amsterdam, 1980), p. 619.
  - [19] Y. N. Demkov and V. N. Ostrovsky, *Zero-Range Potentials and their Applications in Atomic Physics* (Plenum, New York, 1988).
  - [20] J. P. Gauyacq, *J. Phys. B* **13**, 4417 (1980).
  - [21] J. P. Connerade and V. N. Ostrovsky, *J. Phys. B* **35**, L475 (2002).
  - [22] R. Mayol and F. Salvat, *At. Data Nucl. Data Tables* **65**, 55 (1997).
  - [23] J. H. Macek, S. Yu. Ovchinnikov, and E. A. Solovev, *Phys. Rev. A* **60**, 1140 (1999).
  - [24] W. Schmitt, R. Moshhammer, F. S. C. O'Rourke, H. Kollmus, L. Sarkadi, R. Mann, S. Hagmann, R. E. Olson, and J. Ullrich, *Phys. Rev. Lett.* **81**, 4337 (1998).
  - [25] C. R. Liu and A. F. Starace, *Phys. Rev. Lett.* **62**, 407 (1989).
  - [26] R. O. Barrachina, *Nucl. Instrum. Methods Phys. Res. B* **124**, 198 (1997).
  - [27] R. O. Barrachina, *J. Phys. B* **23**, 2321 (1989).
  - [28] L. Viktor, L. Sarkadi, F. Penent, A. Bader, and J. Palinkas, *Phys. Rev. A* **54**, 2161 (1996).
  - [29] J. P. Grouard, V. A. Esaulov, R. I. Hall, J. L. Montmagnon, and V. N. Tuan, *J. Phys. B* **19**, 1483 (1986).
  - [30] F. Penent, J. P. Grouard, J. L. Montmagnon, and R. I. Hall, *J. Phys. B* **24**, 173 (1990).
  - [31] R. von Hahn *et al.*, *Rev. Sci. Instrum.* **87**, 063115 (2016).
  - [32] R. Moshhammer, M. Unverzagt, W. Schmitt, J. Ullrich, and H. Schmidt-Böcking, *Nucl. Instrum. Methods Phys. Res. B* **108**, 425 (1996).

- [33] J. Ullrich, R. Moshhammer, A. Dorn, R. Dörner, L. P. H. Schmidt, and H. Schmidt-Böcking, *Rep. Prog. Phys.* **66**, 1463 (2003).
- [34] R. Moshhammer, W. Schmitt, J. Ullrich, H. Kollmus, A. Cassimi, R. Dörner, O. Jagutzki, R. Mann, R. E. Olson, H. T. Prinz, H. Schmidt-Böcking, and L. Spielberger, *Phys. Rev. Lett.* **79**, 3621 (1997).
- [35] L. P. H. Schmidt, M. S. Schöffler, K. E. Stiebing, H. Schmidt-Böcking, R. Dörner, F. Afaneh, and T. Weber, *Phys. Rev. A* **76**, 012703 (2007).
- [36] P. Balling, P. Kristensen, H. Stapelfeldt, T. Andersen, and H. K. Haugen, *J. Phys. B* **26**, 3531 (1993).
- [37] S. Trajmar, D. F. Register, and A. Chutjian, *Phys. Rep.* **97**, 219 (1983).
- [38] M. J. Brunger, *Int. Rev. Phys. Chem.* **36**, 333 (2017).
- [39] K. Fedus, *Atoms* **9**, 91 (2021).
- [40] G. J. Lockwood and E. Everhart, *Phys. Rev.* **125**, 567 (1962).
- [41] R. Schuch, M. Schulz, Y. S. Kozhedub, V. M. Shabaev, I. I. Tupitsyn, G. Plunien, P. H. Mokler, and H. Schmidt-Böcking, *Phys. Rev. A* **101**, 042701 (2020).
- [42] X. Shi, T. M. Stephent, and P. D. Burrow, *J. Phys. B* **26**, 121 (1993).
- [43] F. Carelli, K. Fedus, and G. Karwasz, *Atoms* **9**, 97 (2021).
- [44] M.-Y. Song, H. Cho, G. P. Karwasz, V. Kokoouline, and J. Tennyson, *Eur. Phys. J. D* **77**, 105 (2023).